Independent Pixel and Monte Carlo Estimates of Stratocumulus Albedo

ROBERT F. CAHALAN, WILLIAM RIDGWAY,* AND WARREN J. WISCOMBE

NASA/Goddard Space Flight Center, Laboratory for Atmospheres, Greenbelt, Maryland

STEVEN GOLLMER AND HARSHVARDHAN

Department of Earth and Atmospheric Sciences, Purdue University, Lafayette, Indiana

(Manuscript received 13 September 1993, in final form 1 June 1994)

ABSTRACT

Monte Carlo radiative transfer methods are employed here to estimate the plane-parallel albedo bias for marine stratocumulus clouds. This is the bias in estimates of the mesoscale-average albedo, which arises from the assumption that cloud liquid water is uniformly distributed. The authors compare such estimates with those based on a more realistic distribution generated from a fractal model of marine stratocumulus clouds belonging to the class of "bounded cascade" models. In this model the cloud top and base are fixed, so that all variations in cloud shape are ignored. The model generates random variations in liquid water along a single horizontal direction, forming fractal cloud streets while conserving the total liquid water in the cloud field. The model reproduces the mean, variance, and skewness of the vertically integrated cloud liquid water, as well as its observed wavenumber spectrum, which is approximately a power law. The Monte Carlo method keeps track of the three-dimensional paths solar photons take through the cloud field, using a vectorized implementation of a direct technique. The simplifications in the cloud field studied here allow the computations to be accelerated. The Monte Carlo results are compared to those of the independent pixel approximation, which neglects net horizontal photon transport. Differences between the Monte Carlo and independent pixel estimates of the mesoscale-average albedo are on the order of 1% for conservative scattering, while the plane-parallel bias itself is an order of magnitude larger. As cloud absorption increases, the independent pixel approximation agrees even more closely with the Monte Carlo estimates. This result holds for a wide range of sun angles and aspect ratios. Thus, horizontal photon transport can be safely neglected in estimates of the area-average flux for such cloud models. This result relies on the rapid falloff of the wavenumber spectrum of stratocumulus, which ensures that the smaller-scale variability, where the radiative transfer is more three-dimensional, contributes less to the plane-parallel albedo bias than the larger scales, which are more variable. The lack of significant three-dimensional effects also relies on the assumption of a relatively simple geometry. Even with these assumptions, the independent pixel approximation is accurate only for fluxes averaged over large horizontal areas, many photon mean free paths in diameter, and not for local radiance values, which depend strongly on the interaction between neighboring cloud elements.

1. Introduction

The purpose of this paper is to consider the 3D radiative effects of cloud inhomogeneity, as prescribed by a "bounded cascade" fractal model, which simulates the horizontal variability observed in marine stratocumulus clouds. This model was introduced in earlier work (Cahalan et al. 1990; Cahalan and Wiscombe 1993) and was based on studies of cloud fractal properties (Cahalan and Joseph 1989; Cahalan and Snider 1989). It was recently used to compute the bias associated with plane-parallel estimates of area-averaged albedo (Cahalan et al. 1994, hereafter C1). Barker (1992) discussed the determination of this plane-parallel albedo bias from in situ cloud measurements. In C1 it was estimated from surface microwave measurements of liquid water path in California marine stratocumulus and found to be approximately 0.1, or 15% of the typical albedo of 0.6, and generally larger than the bias associated with cloud fraction for the available summertime observations. (We consistently follow the convention of C1 that the absolute bias is expressed as a fraction, while the relative bias is given in percent.) Cahalan et al. (1994) employed the independent pixel approximation (IPA), which neglects net horizontal photon transport. Here the IPA results are compared to those derived from 3D Monte Carlo simulations of the cloud radiative processes. The resulting errors in the IPA depend on the scaling properties of the bounded model, which have been studied in detail by Marshak

* Permanent affiliation: Applied Research Corporation, Landover, Maryland.

Corresponding author address: Dr. Robert F. Cahalan, Code 913, Laboratory for Atmospheres, Goddard Space Flight Center, Greenbelt, MD 20771.

et al. (1994) and compared to other fractal models in Davis et al. (1994).

For cloudy atmospheres, the problem of computing radiative fluxes at visible and near-IR wavelengths defies easy or analytic solutions. Cloud multiple scattering, when combined with vapor and droplet absorption processes, is traditionally modeled using one or more simplifying assumptions: namely, that 1) a cloud layer is plane parallel in extent, 2) a cloud layer is homogeneous in composition, and 3) water vapor and/or droplet absorption is negligible or divisible into relatively few gray spectral bands. With such assumptions the radiative transfer problem can be solved by application of well-established procedures such as discrete ordinates (Chandrasekhar 1960) or adding/doubling methods (Hansen 1971; Hansen and Travis 1974; King 1983). Extensions of these "exact" methods to more general cloud geometries (e.g., Stephens 1988a,b) incur substantial penalties in terms of computational effort and numerical complexity, though simple extensions short of full Monte Carlo simulation have been recently applied to advantage (e.g., Evans 1993; Gabriel et al. 1993).

The IPA is perhaps the simplest extension of plane-parallel radiative transfer. It ignores net horizontal photon transport, as does plane parallel, but includes horizontal inhomogeneities in the cloud parameters. IPA computations require knowledge of the one-point probability distributions of cloud parameters, as well as plane-parallel results for parameter values having significant probability. This approach was used in Ronnholm et al. (1980), Harshvardhan and Randall (1985), Stephens et al. (1991), and a wide variety of remote sensing studies. These studies, however, did not estimate the *errors* in the IPA, which requires a model for the *spatial pattern* of the inhomogeneities. An early discussion of such errors based on an additive (normal) random surface model is in Mullamaa et al. (1975). More recently there has been increasing evidence that liquid water in clouds has a multiplicative lognormal-like structure, with power-law structure functions and highly skewed probability distributions. Cahalan et al. (1994) found that the albedo bias of bounded cascades is sensitive to the skewness, and thus the nonnormal nature, of the liquid water distribution by assuming the IPA. Here we show that the results of C1 are valid by showing that the IPA accurately estimates the albedo bias of bounded cascades, even though the IPA errors are often locally quite large. We also confirm that the IPA does not provide a good approximation for the albedo bias of *singular* cascades, as found earlier by Cahalan (1989) and Lovejoy et al. (1990).

Monte Carlo radiative transfer models have become common tools whose algorithmic details are infrequently documented in the scientific literature. The Monte Carlo technique is discussed in some generality for radiative transfer applications by House and Avery (1969). Specific procedures for basic forward and backward Monte Carlo simulations are well described by Kattawar (1979). A mathematically rigorous treatment can be found in Marchuk et al. (1980). More recently, special techniques for uniform sampling and more rapid convergence in moderately thick clouds have been documented by O'Brien (1992).

A number of Monte Carlo studies have addressed atmospheric problems, including cloud geometries other than plane parallel. Harshvardhan (1991) has reviewed some of these. McKee and Cox (1974), Davies (1978), Weinman and Harshvardhan (1982), and Davies et al. (1984) focused on the effects of finite cloud extent and cloud sides on cloud field albedo, bidirectional reflectivity, and absorption. In these studies, clouds were generally assumed to be homogeneous Euclidean objects such as cubes. Coakley and Kobayashi (1989) studied the albedo biases associated with such broken cloud fields. Cahalan (1989) discussed Monte Carlo albedo estimates for a multifractal model, the "singular model," showing that cloud fields with horizontally variable liquid water always have lower average albedo than plane-parallel clouds having the same total liquid water, and that the average albedo is insensitive to variability on scales smaller than a photon mean free path. Lovejoy et al. (1990) studied the asymptotic properties of a multifractal cloud in the limit of large optical thickness, showing that the transmittance approaches zero more slowly than for plane-parallel clouds. Kobayashi (1991) confirmed that finite clouds and clouds with horizontal variability have lower reflectance than uniform clouds with comparable liquid water. Stephens et al. (1991) considered the complementary situation of a layer that is horizontally uniform but statistically distributed in the vertical. Barker and Davies (1992) compared the power spectra of satellite radiances with those of radiances derived from Monte Carlo to explain observed scaling violations.

The method of Monte Carlo simulation is a well-established tool for studying specific cloud geometries, particularly finite three-dimensional clouds. The method's principal advantage is that results are faithful to the detailed physical cloud model, so that flux or radiance estimates are made without further approximations being applied to the transfer equation. Other methods, such as plane-parallel or discrete angle methods, while simplifying the radiative transfer problem, introduce approximations tending to reduce the degrees of freedom of the radiation field and thus fail to fully treat cloud inhomogeneity, an essential theme of this study. The Monte Carlo method has two distinct disadvantages, however: 1) calculations can be computationally expensive, and 2) computed radiative quantities are subject to statistical error. These disadvantages are overcome by appropriate use of parallel/vector processing computer platforms and by development of techniques to reduce the computational demands of using fine geometrical grids, as discussed in

detail below. Estimates of the statistical uncertainties for typical simulations will also be given.

The plan of this paper is as follows. Section 2 summarizes aspects of the fractal cloud model implemented here. Section 3 discusses some details of the Monte Carlo radiative transfer model. Section 4 summarizes the results of the full 3D radiative calculations and emphasizes comparison with the simpler IPA. Section 5 discusses our general conclusions. Finally, appendix A documents various computational enhancements, which greatly improve model efficiency, and appendix B details the statistical errors in both the Monte Carlo and fractal aspects of the model.

2. Fractal cloud geometry

The fractal cloud model discussed in C1 invokes a random cascade process to distribute liquid water nonuniformly across many (typically 2^{12}) horizontal pixels. (As we will see, what is called a "pixel" here is actually an infinitely long cloud street, but in the spirit of remote sensing, we will take it to mean the smallest resolved cloud element.) The drop distribution is assumed uniform, so that the scattering vertical optical thickness is linearly proportional to the vertically integrated liquid water path in each pixel. The cloud is constrained to lie in a horizontal slab between planar upper and lower boundaries, the cloud top and base. Zero surface albedo is assumed, and the side boundaries are periodic, so that photons exiting one side enter the other. The cloud field scattering optical thickness is a random function of horizontal position, with statistical properties that depend on the mean vertical scattering optical thickness and two fractal parameters. The fractal parameters are determined by observations of 1) the variance of the logarithm of vertically integrated cloud liquid water, and 2) the exponent of the power spectral density function of the liquid water, which determines how the variance is partitioned in wavenumber. The random cascade process redistributes the cloud liquid water inhomogeneously in one direction, while leaving it uniform in the other horizontal direction, creating a "cloud street" structure like that in Fig. 1. This is a particular cloud field realization with specified total liquid water. Other cloud field realizations are generated using different random number sequences for the cascade process. In order to characterize the average radiative effects, the Monte Carlo radiative transfer model is applied to each cloud field realization, and the resulting fluxes are averaged over all realizations.

The cascade begins with a slab of uniform vertical thickness, with a large but finite horizontal width and infinite horizontal length, and proceeds as follows: the slab is divided in half lengthwise; one half is chosen at random with equal probability, and a fraction $f_0 = f$ of liquid water is transferred into that half from the other half. The same process of subdivision and transfer is then carried out within each half, transferring a reduced fraction $f_1 = fc$, with $c < 1$, between each pair of quarter slabs; the same is then done within each quarter, transferring $f_2 = fc^2$ between eighths, and so on. The microphysical properties are not varied so that the scattering optical thickness in each section is proportional to the liquid water there. In the bounded model the parameter c is chosen to be $2^{-1/3} \approx 0.8$, which gives a $k^{-5/3}$ power spectrum, and the parameter f is determined by the variance of the logarithm of the vertically integrated cloud liquid water, as discussed in detail in C1. A typical value is $f = 0.5$, based on observations of California marine stratocumulus. In the singular model we set $c = 1$, so that the same fraction is transferred at each cascade step. As shown in C1, the statistical moments develop essential singularities in the limit $c \to 1$, so that the power spectrum and other singular model properties cannot be obtained from the bounded model by analytic continuation and are qualitatively distinct.

The same approach can generate variability in the other spatial directions. For a 2D cascade, one begins with a slab that is large but finite in both horizontal directions. It is divided in half along both length and width, making four equal quarter slabs. One quarter slab is chosen at random, and a fraction $f_0 = f$ is transferred to one of the other three, also chosen at random, and the same fraction is transferred between the remaining two, with the direction chosen at random. The same two values of liquid water obtained at the first step of the 1D cascade appear *twice* at the first step of the 2D cascade. The process is continued by treating each quarter slab the same way, transferring $f_1 = fc$ among sixteenths. Each value occuring at the nth step of the 1D cascade occurs at 2^n locations in the 2D cascade, thus generating the same one-point probability distribution and the same IPA fluxes. Monte Carlo fluxes for a 2D cascade are shown in Cahalan (1994). Vertical variability may be generated in the same way, with either a uniform or linearly increasing mean vertical profile. In section 4 we give results for the 1D model and then qualitatively discuss our expectations for 2D and 3D generalizations.

Table 1 compares the bounded and singular models described above. In the singular model, the fractions f_n do not vary with the cascade step n, and in the limit $n \to \infty$ the liquid water is confined to a set of singularities of various strengths, for which one can define a dimension function and singularity spectrum, which are analytic functions of the parameter f. The optical thickness distribution is unbounded. The power spectrum in the singular model follows a power law with an exponent that is a simple function of f, but always between 0 and -1. [This model was studied in Cahalan (1989).] By contrast, in the bounded model the fractions f_n decrease with the cascade step, produce an optical thickness distribution strictly bounded both above and below, and a power-law spectrum with an exponent

FIG. 1. Vertical cross section through a cloud field that has several cloud streets identical in geometry and microphysical properties but different in vertical optical thickness. The streets represent the smallest resolved elements after a certain number of cascade steps of a fractal model and are referred to in the text as pixels. In the realization shown here, the optical thicknesses were assigned by three iterations of the cascade process, with horizontal average thickness $\tau_v = 16$ and fractal parameter $f = 0.6$. The reflectance R shown with each optical thickness is that of the independent pixel approximation, which neglects net horizontal photon transport. Also shown are possible paths a photon can take during a Monte Carlo simulation, which can generate deviations from the independent pixel reflectances.

that is independent of f and approximately equals $-\frac{5}{3}$ when $c \approx 0.8$, as observed (Cahalan and Snider 1989; see also Davis et al. 1994). These results are derived in C1, and a detailed discussion of the scaling properties of the bounded model is given in Marshak et al. (1994).

Our use of a multiplicative cascade to generate cloud structure has a twofold motivation: 1) the mesoscale

TABLE 1. Comparison of cascade models.

Quantity	Singular model	Bounded model
Cascade fractions	$f_n = \text{const} = f$	$f_n = fc^n$, $c \approx 0.8$
Maximum thickness	$\tau_{max} \to \infty$	$\tau_{max} \leq \tau_v \exp[f/(1-c)]$
Wavenumber spectrum	$S(k) \sim k^{-1}$ or flatter	$S(k) \sim k^{-5/3}$
Plane-parallel bias	20%	15%
Independent pixel bias	−10%	≤1%

variability in cloud liquid water is thought to be generated by a two-dimensional upscale energy cascade forced by small-scale convection (see, e.g., Gage and Nastrom 1986), and 2) the mesoscale-averaged radiative properties that we wish to derive depend on the moments of the optical thickness distribution, and in particular its *skewness,* which cannot be generated by an additive model. For example, a simple Fourier series with random amplitudes could generate the observed $k^{-5/3}$ spectrum, but the liquid water would then have a Gaussian distribution. The cascade model also generates a $k^{-5/3}$ spectrum but has the advantage of producing a skewed lognormal-like distribution, which more closely resembles the observations (see C1).

Figure 1 shows a cross section through one realization of a bounded cascade and three relatively simple photon paths. The realization was generated from three cascade steps, since $2^3 = 8$ values of scattering optical thickness are shown. Photon A scatters in the forward hemisphere three times then exits downward; photon B scatters backward once then exits upward; and photon C enters the cloud behind the plane of the paper, scatters sideways into the plane of the paper, then forward once and backward once, and finally exits the cloud upward. According to this three-photon sample, the cloud reflectivity is 2/3 and the transmissivity is 1/3. Results given below are based on 4×10^6 photons, distributed over $2^{12} = 4096$ pixels with scattering optical thicknesses generated from 12 cascade steps. Most photon paths are much more complex than those shown here.

Table 2 summarizes the meaning and typical values of various parameters used in this paper. The table gives the mean vertical scattering optical thickness τ_v and total horizontal cloud field optical thickness τ_h. This implies a mean single-pixel horizontal scattering optical thickness of $\tau_h/4096$, since there are 4096 pixels. The pixel aspect ratio is defined as the ratio of vertical to horizontal pixel size, which is also the ratio of vertical to horizontal pixel scattering optical thickness. All pixels within the cloud have the same geometrical size and aspect ratio, typically between 1 and 100. Single-pixel horizontal and vertical scattering optical thickness scale with the cascade model scattering opacity function. Thus, the optical thickness values can be translated into physical units by assuming a value for the extinction, typically 30 km^{-1}.

3. Simulation model: Direct method

a. *Concept of local optical density, phase function, solar parameters*

The first task in simulating the radiation field is to specify cloud droplet spatial structure. For this study, we have assumed that horizontal inhomogeneity is reflected solely in the *density* of cloud droplets, and thus their size distribution is uniform. The scattering phase

TABLE 2. Primary quantities and symbols.

Quantity	Symbol	Typical values
	fractal cascade	
Variance parameter	f	0.5 (0.8 global)
Spectral parameter	c	0.8 (for $k^{-5/3}$ spectrum)
	macrophysical	
Sun angles	θ_0, ϕ_0	60°, 0°
Mean vertical optical thickness	τ_v	1–16
Total horizontal optical thickness	τ_h	409.6–40 960
Pixel vertical optical thickness	τ	0.1–100
Pixel horizontal optical thickness	$\tau_h/4096$	0.1–10
Pixel aspect ratio	$\tau_v/(\tau_h/4096)$	1–100
Mean vertical liquid water path	$W = \tau_v/0.15$	10–100 g m^{-2}
	microphysical	
Asymmetry parameter	g	0.85
Single scattering albedo	ω_0	0.9–1.0
Scattering angles	Θ, Φ	0°–180°, 0°–360°
	cloud/solar flux ratios	
Reflectance, transmittance, absorptance	R, T, A	0.5, 0.5, 0.0
Independent pixel (ip) estimates	R_{ip}, T_{ip}, A_{ip}	0.5, 0.5, 0.0
Plane-parallel (pp) estimates	R_{pp}, T_{pp}, A_{pp}	0.6, 0.4, 0.0
pp biases ($R_{pp} - R_{ip}$, etc.)	$\Delta R_{pp}, \Delta T_{pp}, \Delta A_{pp}$	0.1, −0.1, 0.0
ip biases ($R_{ip} - R$, etc.)	$\Delta R_{ip}, \Delta T_{ip}, \Delta A_{ip}$	0.01, 0.01, 0.01

function and single scattering albedo are invariant, while cloud optical thickness is highly variable.

By stopping after a finite number of cascade steps (typically 12), the fractal model determines a length scale over which droplet density is nearly constant and the local scattering optical density function is well defined. The spatial structure underlying the Monte Carlo model therefore consists of rectilinear pixels, which are small enough to have uniform cloud optical properties within each pixel. This assumption of homogeneity at small scales seems reasonable but should be tested against better in situ data than has so far been available. The pixels are fixed in size with a specified vertical to horizontal aspect ratio. The cloud field is one pixel thick, that is, uniform in the vertical direction between cloud base and top but with horizontal inhomogeneity embodied in the cloud scattering optical density, which varies pixel by pixel in one horizontal direction. (The scattering optical density function is based on the fractal model but, for the purposes of the Monte Carlo simulation, could be any function of one horizontal coordinate with the constraint that it be slowly varying on the scale of a single pixel's horizontal extent. The fractal cascade model is just one such cloud representation.)

Radiative calculations are done using a droplet single scattering phase function specified by a Henyey–Greenstein function with asymmetry parameter 0.85. Solar radiation uniformly illuminates the cloud top and is taken to be incident at some angle from the zenith (typically 60°) in the vertical plane defined by the direction of cloud inhomogeneity. This choice of azimuthal angle means that each photon moves, at the outset, in the direction of greatest horizontal inhomogeneity, allowing it to sample regions of varying scattering optical density. The opposite choice, an azimuth angle corresponding to the horizontal direction with uniform cloud properties, is not chosen because it would exaggerate cloud street effects, giving results less representative of realistic 3D variability.

b. *Forward photon simulation model*

The Monte Carlo method employed here is a direct method, that is, a straightforward simulation of photon trajectories. It is particularly well suited to fast calculations of radiative fluxes to which a moderate to large percentage of all photon trajectories actually contribute, as in the determination of mean cloud field albedo. Photons enter initially at cloud top; an equal number are incident on each cloud pixel, and the actual point of incidence within each pixel top is randomly selected. Each photon proceeds through a series of scatters to emerge from either cloud top or cloud base. (Those still remaining in the cloud after 500 scatters are assumed to exit the pixel within which they last scattered, with equal probability of exiting up or down, as discussed below with regard to Fig. 4.) The simulation is conservative; that is, no photons are explicitly absorbed or otherwise terminated within the cloud. Instead, the scattering optical pathlength traveled by each photon within the cloud is recorded so that this quantity, together with the single scatter albedo, can be used to compute the absorption pathlength and thereby estimate the probability of absorption by the cloud at any wavelength. We first consider conservative scattering; the treatment of nonconservative clouds is discussed later.

Within the cloud, the Monte Carlo photon simulation proceeds as a sequence of repeated primitive events. These are of three distinct types: 1) crossing a pixel boundary, 2) termination of a straight path segment at a scatter event, and 3) emergence from a scatter event with a new trajectory. While events of type 2 and 3 are actually part of a single physical scattering process, this event structure serves to emphasize the simplicity of the Monte Carlo simulation. Photons exiting the cloud entirely are a special case of event 1.

The simulation proceeds by determining the distance to the next scatter point and the direction of travel after scattering then repeating both steps in succession. The scattering optical pathlength τ between successive scatters is a random variable chosen from an exponential distribution having the simple form

$$\rho(\tau) = \exp(-\tau). \tag{3.1}$$

Equivalently, in terms of the probability X that the scattering optical path is greater than τ,

$$\tau = -\log(X), \tag{3.2}$$

where X is selected from a uniform distribution on the interval $0 < X < 1$. Thus, a single random number X locates the next scattering event by tracing the photon trajectory through a sufficient number of pixels to accumulate the corresponding scattering optical pathlength τ. [We typically use the system-provided random number generator but sort to eliminate correlations. Press et al. (1992) give an excellent review of various random number techniques.]

The included angle of scattering Θ is determined by identifying the cumulative integral of the Henyey–Greenstein phase function with a second random number Y, again uniformly distributed on the unit interval, $0 < Y < 1$. This gives

$$\cos(\Theta) = \frac{1 + g^2 - [(1 - g^2)/(1 - g + 2gY)]^2}{2g}. \tag{3.3}$$

Finally, the scattering azimuthal angle Φ is chosen randomly using a third random number Z with

$$\Phi = 2\pi Z, \tag{3.4}$$

and Z uniformly distributed on the interval $0 < Z < 1$. These values of Θ and Φ are defined with respect to the incident photon direction. A simple rotation gives

their equivalents in the coordinate system of the cloud field. Once the new direction is known with respect to the cloud, its projection onto the normals defining each surface of the cloud pixel determines which face the photon will exit.

As each event occurs, key quantities are recorded, including photon position, direction, and accumulated pathlength; a logical flag marks photons that have exited at the upper or lower boundary. In practice, in order to take advantage of vector computer capabilities, it is better to treat batches of many photons together. The entire batch is followed through successive orders of scattering until most have exited the cloud. The exiting photons are "frozen" in place at the cloud base or cloud top to await completion of the remaining photon trajectories.

c. *Results obtained from binning photons on exit*

Cloud field albedo in the nonabsorbing case is estimated by counting all photons that emerge from the cloud top, where each photon represents a fixed fraction of the incident solar flux. Exiting photons are binned according to exit position, emergent direction, and scattering optical pathlength traveled within the cloud. (Other quantities such as entry position, order of scatter, and physical distance traveled are possible alternate criteria for binning.) Because each photon represents a single flux quantum and all contribute to conservative reflection or transmittance, the simulation is quite efficient in modeling cloud field albedo and the radiative energy budget. The spatial and angular distribution of scattered radiation is also computed based on individual spatial/angular bin fluxes, but these are subject to much greater statistical errors associated with proportionately smaller photon samples.

d. *Treatment of nonconservative medium*

Since the Monte Carlo model outlined above is conservative, all photons that enter the cloud top exit somewhere, contributing to the reflected or transmitted fluxes. All photons carry the same fraction of the incident flux throughout their lifetimes. The primary advantages of this method are its computational simplicity and that statistical errors are easily estimated. All flux estimates are represented by simple counting, with errors generally of order $n^{-1/2}$, where n photons contribute to a flux estimate, as discussed in detail in appendix B.

Absorption is not simulated explicitly because that would require new simulations for each absorbing wavelength. Droplet and vapor absorption vary with wavelength by many orders of magnitude, while scattering cross section and phase function are much less sensitive to wavelength. A direct Monte Carlo model with droplet or vapor absorption would require repeated simulations using different single scattering albedos. Instead, we follow Davies et al. (1984), who observed that for flux estimates each photon exiting the medium should be weighted in proportion to its actual probability of survival, which is simply a function of the absorption pathlength traversed within the cloud. Thus, conservative model flux estimates are modified at each wavelength by photon survival probability. The reflectance (reflected flux over incident flux) is

$$R = \sum_i \exp\left[-\frac{1-\omega_0}{\omega_0}\tau_i\right] \Big/ F_0, \qquad (3.5)$$

where single scattering albedo ω_0 is implicitly a function of wavelength, the index i denotes individual photons that contribute to cloud reflectance by exiting at cloud top, τ_i is the scattering optical pathlength traversed by photon i, and F_0 is the incident solar flux. The absorption optical pathlength has been computed from the scattering optical pathlength using the ratio of absorption to scattering $(1-\omega_0)/\omega_0$. Photons exiting with comparable scattering optical pathlengths will have the same probability of survival, so they are naturally grouped together to form a pathlength distribution function $p(\tau)$. Reflectance at each wavelength is determined from this distribution function according to

$$R = \int p(\tau) \exp\left[-\frac{1-\omega_0}{\omega_0}\tau\right] d\tau. \qquad (3.6)$$

Hence, reflectance at all wavelengths is determined from the pathlength distribution of a single Monte Carlo simulation.

4. Results

For convenience, we will separate the total bias in the area-average reflectance into two components, as follows:

$$\text{bias} = R_{\text{pp}} - R = \Delta R_{\text{pp}} + \Delta R_{\text{ip}},$$

where the first term on the rhs, the plane-parallel bias, is given by the plane-parallel reflectance R_{pp} minus the IPA reflectance R_{ip} and was discussed in C1 and shown to be quite large. We will focus here on the second term, the independent pixel bias, given by the IPA reflectance minus the area-average reflectance R, as estimated by Monte Carlo. We will see that this bias is much smaller than the plane-parallel bias, but only when averaged over a complete cloud field, 100 km or more in extent, and not for individual pixels.

Before presenting results for fully inhomogeneous clouds, it is important to have a clear idea of the impact of 1) Monte Carlo noise and 2) horizontal photon transport. To that end, let us first consider the Monte Carlo reflectance estimates for a cloud field with a small number of uniform, plane-parallel regions, where the "true" reflectance in each region is known from plane-parallel theory. In particular, consider a plane-parallel slab consisting of 4096 geometrically identical pixels

with mean vertical optical thickness $\tau_v = 16$ and horizontal optical thickness 1.6 (i.e., aspect ratio 10), so that the total horizontal optical thickness is $\tau_h = 6553.6$. Assuming a typical extinction of 30 km^{-1}, the physical dimensions of the cloud are thickness = 533 m and width = 218 km. By taking 3 cascade steps of the bounded model with $f = 0.6$, $c = 0.8$, we divide this into eight cloud streets each 27.3 km wide, one realization of which is shown in Fig. 1. Each cloud street has identical microphysical properties, with $\omega_0 = 1.0$, Henyey–Greenstein phase function with $g = 0.85$, and the sun at $\theta_0 = 60°$, $\phi_0 = 0°$.

Figure 2a shows the reflectances of the cloud described above, averaged over 8-pixel cells, as estimated by the Monte Carlo method discussed in the previous section, using 4×10^6 photons, or nearly 8000 photons per cell. Away from their edges, the cloud streets should have constant reflectances equal to their plane-parallel values. If we compute the plane-parallel reflectance from the optical thickness of each cell and subtract the Monte Carlo reflectance, we obtain the independent pixel bias, which is the lower line in Fig. 2a. The small fluctuations seen here, those not near the edges of the cloud streets, are due to Monte Carlo noise. As shown in appendix B, the standard deviation of this noise decreases with n = the number of photons/pixel as $n^{-1/2}$ so that averaging over 8 pixels decreases the standard deviation by a factor of $\sqrt{8} \approx 3$, to the observed value of ≈ 0.01. Averaging over all 512 cells would further reduce this by a factor of $\sqrt{512} \approx 23$, to less than 2% of the 0.09 plane-parallel albedo bias estimated in C1.

Figure 2a shows dramatic deviations from the IPA estimates at the cloud street edges. For example, the second street from the right has an average reflectivity of ~0.9 but at the sunward edge the reflectivity exceeds 1. Similarly, the two other streets, which are brighter than their neighbors, also have enhanced brightness at their sunward edges. Each of these brightness enhancements is also accompanied by a darkening at the edge opposite the sun. Since each downward spike in the IP bias has its accompanying upward spike, the edge effects tend to cancel out in the overall horizontal average (though not identically), so that the independent pixel bias is relatively small. Thus, the IPA produces a highly accurate average reflectance, even though the local values have large errors.

Let us now consider a fully inhomogeneous cloud. Figure 2b shows the reflectivity of one realization of the bounded model after 12 cascades, computed with the same parameters as in Fig. 2a. The sun is again 60° to the left of the zenith, and the upper curve shows the Monte Carlo reflectivity, while the lower curve is the independent pixel bias. This cloud was generated from the one in Fig. 2a by simply continuing the cascade for nine further steps. Thus, the Monte Carlo noise in Fig. 2b has the same magnitude as that of Fig. 2a, but now much larger fluctuations of both signs appear in the

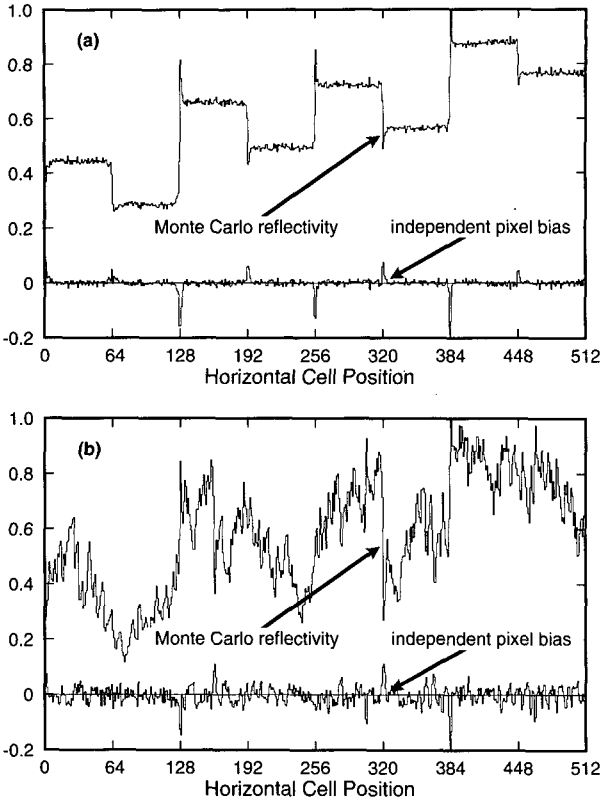

FIG. 2. Monte Carlo pixel reflectance and independent pixel bias for (a) the eight cloud streets of Fig. 1 and (b) 4096 cloud streets. Each cloud street has identical microphysical cloud properties with $\omega_0 = 1.0$, Henyey–Greenstein phase function with $g = 0.85$, and identical geometrical thicknesses but different vertical optical thicknesses τ, with horizontal mean $\bar{\tau} = \tau_v = 16$. The sun is 60° to the left of the zenith. In (a) each street is approximately 30 km wide and consists of 512 identical pixels. Each plotted value in (a) and (b) is an average over cells consisting of 8 pixels. The standard deviation of the Monte Carlo noise decreases with the number of photons/pixel as $n^{-1/2}$, so that averaging over 8 pixels decreases the standard deviation by a factor of almost 3. Overall 4 000 000 photons are tracked.

independent pixel bias over the whole cloud, due to the large number of edges that occur throughout the cloud. As in Fig. 2a, the negative spikes associated with the sunward edges are always accompanied by positive spikes, making the horizontal-mean independent pixel bias closely approach zero. In this case, the overall independent pixel bias ± the standard deviation is -0.0038 ± 0.033, which is 0.66% ± 5.7% of the mean IPA albedo of 0.5743. This should be compared to the plane-parallel albedo bias. Since $R_{pp}(\tau_v = 16) \approx 0.69$ and $R_{ip} \approx 0.57$, the plane-parallel bias ≈0.12, or 17% of the plane-parallel albedo. Thus, the overall independent pixel bias is negligible. Again, however, we caution that the neglect of horizontal photon transport is *not* justified for *local* reflectance values, as is evident from Fig. 2b.

We now consider the horizontal average of the independent pixel bias for a large number of experiments

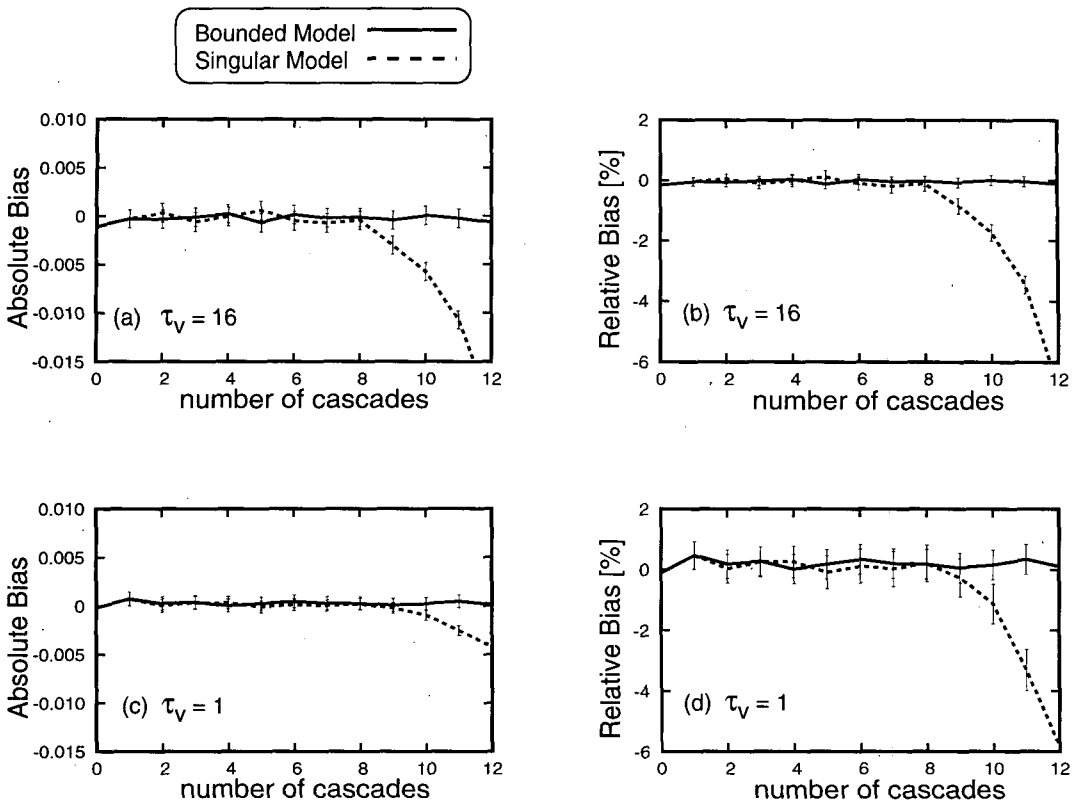

FIG. 3. The horizontal-average independent pixel bias, namely, the area-average reflectance computed by the independent pixel approximation minus that computed by Monte Carlo, versus the number of cascade steps in the fractal cloud model. The singular fractal model has $f = 0.6$, $c = 1$, while the bounded model has $f = 0.6$, $c = 0.8$. For both models, the biases are plotted with a $\pm 2\sigma$ error bar, where σ is the standard deviation of the local pixel reflectances about the mean, so that the width of the error bar gives the 95% confidence interval. Curves in (a) and (b) show the absolute and relative independent pixel bias, respectively, for a mean cloud optical depth of $\tau_v = 16$, while curves (c) and (d) give the analogous results for $\tau_v = 1$. All curves are for conservative scattering ($\omega_0 = 1.0$) with $g = 0.85$, pixel aspect ratio 10, and sun angles $\theta_0 = 60$, $\phi_0 = 0$.

like those illustrated in Fig. 2. Figure 3 shows the independent pixel bias versus the number of cascade steps for the two fractal cascade models described in section 2: the singular model, with $f = 0.6$, $c = 1$, and the bounded model, with the same value of f but with $c = 0.8$. For each of these two models, the independent pixel bias is plotted with an error bar of $\pm 2\sigma$, where σ is the standard deviation of the reflectances about the mean, so that the error bar gives the 95% confidence interval. Curves in panels a and b show the absolute and relative independent pixel bias for a mean cloud optical thickness of $\tau_v = 16$. Curves c and d give the same results for $\tau_v = 1$. All curves are for conservative scattering ($\omega_0 = 1.0$) with $g = 0.85$, pixel aspect ratio $= 10$, and the sun at $\theta_0 = 60$, $\phi_0 = 0$.

For the bounded model, it is clear from Fig. 3 that ΔR_{ip} is always less than 1% for both thick and thin clouds and is therefore negligible compared to ΔR_{pp}. The IPA can therefore safely be used to estimate area-average fluxes for the bounded model. But for the singular model, ΔR_{ip} reaches several percent after 12 cascades and is therefore comparable to ΔR_{pp}. Note that it is negative, which means that the IPA underestimates the reflectivity. For the singular model, then, three-dimensional radiative effects cannot be neglected in estimating area-average fluxes. (Recall, though, that the singular model gives the wrong power spectrum.) The singular model and its relatives have been thoroughly studied previously (see, e.g., Cahalan 1989; Lovejoy et al. 1990), so for the remainder of this paper we restrict our focus to the bounded model.

In order to generalize the results shown in Fig. 3 to the absorptive case, we need the pathlength distribution for conservative scattering, as in Eq. (3.6). Figure 4 illustrates this distribution for the same parameters used in Figs. 3a and 3b. The upper dotted curve is the distribution of pixel optical thicknesses, showing significant fractions between about 0.5 and 200, while the lower dotted curve is the distribution of transmitted photon paths, with no significant fractions between 0.5 and 1.0, but with a significant number above 200. The peak at 500 is an artifact of the imposed cutoff at 500

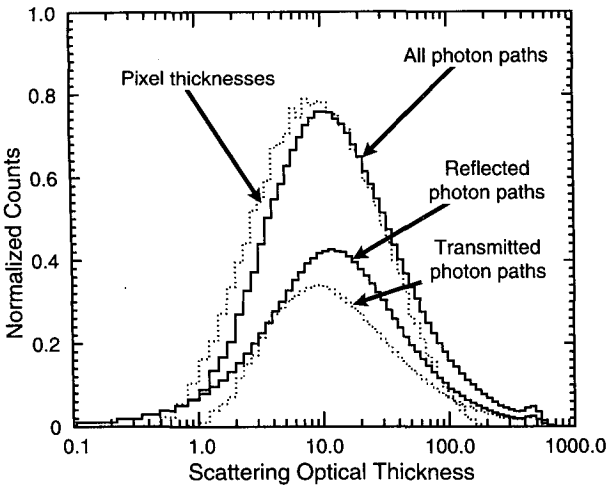

FIG. 4. Pathlength distributions for conservative scattering in the bounded cascade cloud field for the same parameters used in Fig. 3a. The lower dotted curve is for transmitted photons, while the lower solid curve is for reflected photons, and the upper solid curve is the distribution for all photons, which is the sum of the two lower curves. Shown for comparison is the upper dotted curve, which is the distribution of vertical optical thicknesses in the cloud field.

scatters. The lower solid curve is the distribution of reflected photon paths and converges with the distribution of transmitted photons above 200, thus justifying our assumption that "residual" photons are equally likely to exit up or down. The sum of the distributions for reflected and transmitted photons, the two lower curves, of course gives the distribution of all photons, which is the upper solid curve.

By applying Eq. (3.6), with $\omega_0 = 0.99$ and 0.90, to the conservative results shown in Figs. 3a and 3b, with the path distributions shown in Fig. 4, we obtain the absorptive results shown in Fig. 5. As in Fig. 3, this shows the independent pixel bias in the bounded model, but now for nonconservative scattering, showing not only reflectance (R) but also transmittance (T) and absorptance (A). As in Fig. 3, the area-average biases are shown with $\pm 2\sigma$ error bars, giving the 95% confidence interval. Again, as in the conservative case, ΔR_{ip} is always less than 1% for both weak and strong absorption and is therefore negligible compared to ΔR_{pp}. The same is true for the transmittance and absorptance.

Figure 6 shows the independent pixel bias, defined as above, but given now as a function of sun angle, for various aspect ratios, and for conservative scattering. The bias increases with aspect ratio, since this spreads out the local errors horizontally, but the relative error remains less than 1%. The IPA error is larger for larger f (not shown), but it remains small compared to the plane-parallel bias, which also increases with f, as shown in C1. Note that the largest error is at an angle of about 60°, a value typical for the FIRE observations of marine stratocumulus. Even in this case, however, ΔR_{ip} remains much smaller than ΔR_{pp}. For this type of model, then, three-dimensional radiative effects can safely be neglected in estimating the mesoscale-averaged reflectance. Plane-parallel estimates, which depend only on τ_v, can easily be in error by more than 10%, but the error can be reduced to less than 1% by including higher moments of the distribution of pixel optical thickness, as shown in C1.

How might the above results change in the 2D or 3D generalizations of the bounded cascade? The inclusion of vertical or alongstreet variability allows photons to potentially diffuse around peaks in cloud density. As a result, the local errors in the IPA become more spread out than those in Figs. 2a and 2b, without changing the fact that they occur with both signs and tend to cancel when averaged together. As in 1D, the IPA errors tend to be of one sign when then sun is closer to the zenith but are then much smaller locally as well as in the area average. IPA errors for a 2D case are shown in Cahalan (1994). We have not yet included vertical variability but suspect that it is less important than the horizontal in the case of marine stratocumulus, because most of the liquid water is within a photon mean free path of the cloud top, and experience with Monte Carlo computations shows that scales smaller than a photon mean free path are smoothed out by the photon field (Cahalan 1989). This speculation requires further study, which we leave for a later time.

5. Conclusions

In order to obtain what is probably a lower bound for the bias in plane-parallel estimates of mesoscale-averaged cloud albedo, the plane-parallel albedo bias has been estimated for marine stratocumulus clouds, which are the closest cloud type to plane parallel. The estimate employs a model that reproduces the observed mean, variance, and skewness of the vertically integrated cloud liquid water, as well as its observed wavenumber spectrum, which is approximately a power law, $k^{-5/3}$. An earlier paper (Cahalan et al. 1994, referred to here as C1) estimated the bias assuming the independent pixel approximation, or IPA, which neglects horizontal photon transport. The IPA found an absolute bias on the order of 0.09, or 15% of the plane-parallel albedo. The present paper estimates the *additional* bias due to the IPA assumption using a Monte Carlo method and finds it to be less than 0.006, or 1% of the plane-parallel albedo. Thus, for bounded cascade models horizontal photon transport can safely be neglected in estimating the mesoscale-average albedo. For this purpose, the IPA is highly accurate.

Although the bounded model is only weakly inhomogeneous, with the variance strongly concentrated in the largest scales, the resulting 15% albedo bias is still potentially quite significant. If this albedo change were applied globally, the equilibrium surface temperature of the earth would drop below that of the last ice age. Global circulation models currently avoid this

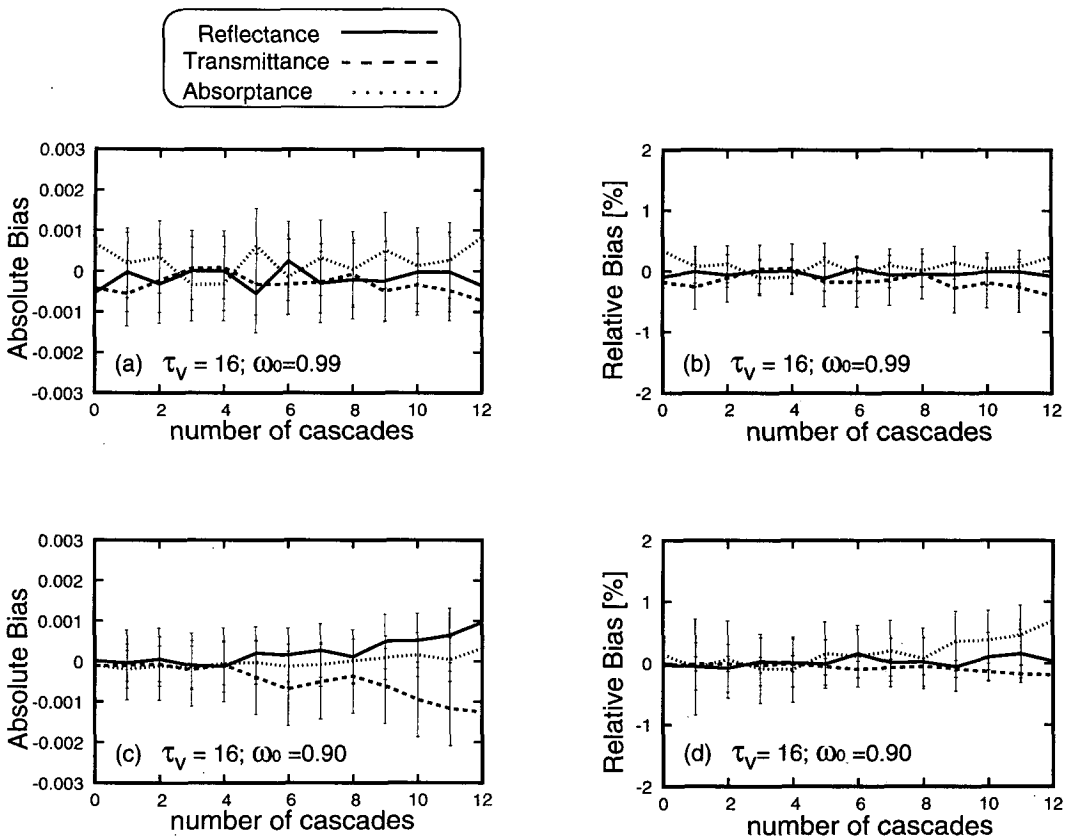

FIG. 5. The independent pixel bias, defined as in Fig. 3, but now for nonconservative scattering ($\omega_0 = 0.99$ and 0.90), showing not only reflectance (R) but also transmittance (T) and absorptance (A) for the $f = 0.6$, $c = 0.8$ bounded model. As in Fig. 3, the area-average curves are shown with $\pm 2\sigma$ error bars, giving the 95% confidence interval for the area average.

problem by simply adjusting cloud albedo directly, without regard to liquid water content. A more physical coupling of radiation and hydrology will require a more realistic adjustment of the plane-parallel albedo estimates. Although a 15% albedo adjustment is probably typical for marine stratocumulus, tropical convective and other more heterogeneous systems are likely to require more radical corrections.

In the IPA, fluxes depend only upon one-point statistics determined by the probability distribution of optical thickness, such as the mean and variance of its logarithm. The accuracy of the IPA decreases as more of the variance is distributed to the smaller scales (so that the wavenumber spectrum falls off more slowly). The singular model, for example, has a k^{-1} or flatter spectrum, and in this case the plane-parallel bias becomes dominated by three-dimensional effects in the limit of infinite cascades. Monte Carlo approaches like the one used here are essential in estimating radiative properties of models like the singular model. Even in that case, however, the IPA is useful in isolating the bias associated with truly three-dimensional effects from that related only to the shape of the probability distribution of optical thickness.

An important observational result discussed in C1 is that the liquid water variability in marine stratocumulus is maximum when the cloud cover is maximum. Within-cloud variability therefore has more impact on the area-averaged albedo than the cloud fraction. One surprising consequence of this is that, during the diurnal cycle of marine stratocumulus, plane-parallel albedo estimates are most in error when the cloud fraction is nearly 100%. That is, the plane-parallel albedo is least accurate when the conventional cloud fraction corrections to it vanish! Clearly, the parameterization of cloudiness in global climate models must include not only cloud fraction, but also the within-cloud fractal structure, which strongly influences the area-averaged albedo and thus the large-scale climate.

While we have most extensively studied one-dimensional (1D) fractal variability shown by the cloud streets in Fig. 1, we have discussed more general bounded cascades having two-dimensional horizontal variability (2D), and both vertical and horizontal vari-

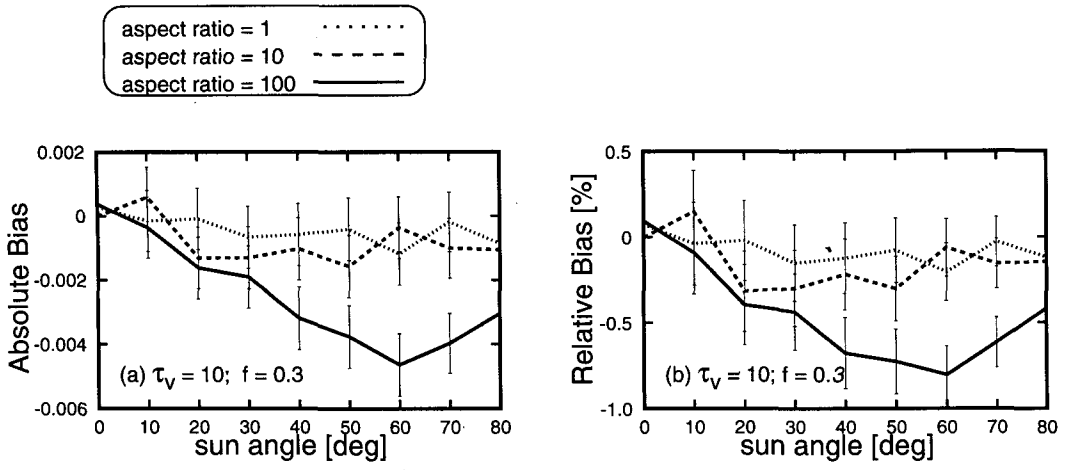

FIG. 6. The independent pixel bias, defined as in Fig. 3, but given here as a function of sun angle, for various aspect ratios (pixel height over width), and for the bounded model with $f = 0.3$, $c = 0.8$. The cloud has $\tau_v = 10$, $\omega_0 = 1$, $g = 0.85$.

ability (3D). For the same parameter values as in Fig. 2, we have verified that the *mean* of the IPA errors remains small in 2D, though local errors become more spread out than in 1D, because of photon diffusion around optically thick regions (see Cahalan 1994). We speculate that vertical variability is less important for stratocumulus, since most liquid water is within a photon mean free path of the cloud top, and previous results find that mean fluxes are insensitive to such variability. For cloud types having significant vertical development, however, we expect large-scale radiative properties to become sensitive to vertical structure. In that case both sides of the energy balance are likely to become sensitive functions of the fractal structure—emissivity as well as reflectivity. The dependence of *net* radiation in deep convective systems on the fractal structure of such systems will be an important question for further research.

Acknowledgments. The authors would like to thank T. Bell, A. Davis, P. Gabriel, A. Marshak, G. Stephens, and S. C. Tsay for helpful discussions. Support from NASA Contracts NAS5-30430 and NAS5-30440, NASA GSRP Fellowship NGT-50963, DOE ARM Grant DE-A105-90ER61069, and NSF Grant ATM-8909870 is gratefully acknowledged.

APPENDIX A

Computational Enhancements

a. Vectorization

Complexity arises in Monte Carlo calculations primarily when geometry is complicated, that is, when photons exploring different cloud regions find very different environments. Due to the relative simplicity of the cloud geometry we have specified and that only a few types of primitive events need to be considered, photons in each region of the cloud and at each order of scatter repeat similar patterns. They move independently of each other and the scattering process depends solely on photon position, direction, and the local scattering opacity. This is an ideal situation for vectorization, and the simulation can be made to proceed rapidly on a vector machine (the Cray-YMP) by grouping photons in batches of several thousand. All move in unison through each successive order of scatter until they exit (none are explicitly absorbed in our model). A list of "still active" photons is maintained and updated at each order of scatter. Photons not appearing on the list are held fixed at their points of exit (effectively ignored). On a vector processing computer, the list serves either to gather active photons into vectors or to mask vectors when updating photon positions, directions, etc.

b. Residual photons

Vectorization has allowed us to process photons at rates 10–100 times faster than comparable scalar simulations. However, there are two obstacles we have encountered that must be overcome in order to vectorize the process successfully. The first, eliminating photons that linger within the cloud after a large number of scatters, is common to all Monte Carlo simulations but is a particular problem for vectorized models. As the still active list becomes short, the advantages of vector processing are eroded, and the simulation expends a disproportionate amount of computational effort on a minute proportion of the radiative flux. We have applied an unsophisticated criterion, simply truncating the calculation at a high order of scatter when the remaining photons represent less than 0.5% of the initial flux. For the purpose of computing cloud field albedo, resid-

ual photons (those still inside) are divided evenly between reflected and transmitted fluxes. Their total pathlengths are set equal to that of their simulated paths to their current positions. The error in pathlength in applying this approximation is not important for the longer paths of these photons.

c. Reducing boundary crossing

A second, more subtle, difficulty in efficient vectorization is presented by regions of low optical density. In a homogenous cloud one could make computational pixels large enough to give photons a significant probability of scatter within each pixel. However, in using a uniform geometrical grid to define a highly inhomogeneous optical density, some regions will contain nearly transparent pixels. Furthermore, since variability in the bounded model is smoother at smaller scales, a transparent pixel typically has many contiguous pixels nearly as (or more) transparent. Photons crossing these transparent regions (particularly those traveling nearly horizontally) will cross many pixel boundaries before reaching their next point of scatter. As a result, much time is spent tracking straight lines through nearly transparent cloud regions. Most photons reach their next scattering point and wait, while a relative few are still crossing boundaries.

We have overcome this problem by reducing the number of boundary crossings. Photons are permitted to cross pairs of adjacent pixels where the combined "superpixel" is defined to have an optical density equal to the average of the two component pixels. There is no approximation in this procedure provided the photon has equal geometrical pathlength in each pixel. Pixel merging is continued in a hierarchical fashion as long as there are some regions where photons are moving across these superpixels.

The pixel merging is done as follows: After a scatter event photons are moved along individual trajectories to the next boundary. Those that fall on a superboundary are held fixed, while those at the middle of superpixels are transmitted along their trajectories to the appropriate boundary. Any photons that would reach a scatter point before the next boundary are left at their positions. The next level of superpixels is defined in the same fashion, based on the current level, and the identical process is repeated, again only for those photons that have not accumulated sufficient optical path to reach the next scatter. Pixel merging is stopped when no photons are moving. At this point the entire process is reversed, superpixels are split, and photons moved to superpixel midpoints, etc., until all photons finally are held at the boundary just before their next scatter point. They traverse to the last scatter through the original pixel structure in order that pathlength is computed correctly over this shorter path segment.

This hierarchical scheme reduces the computational effort from a linear to a logarithmic dependence on the maximum number of boundary crossings. This can be particularly important in cases where some pixels are completely clear. For example, the hierarchical scheme allows us to compare results for a fractal cloud field to other models having finite clouds embedded in a clear atmosphere.

APPENDIX B

Monte Carlo Statistical Errors

a. Plane-parallel example

The direct Monte Carlo method provides estimates of the radiative flux F_r to be measured through any defined surface and prescribed solid angle. Flux estimates are quantized in terms of photon counts, with each photon representing a single flux quantum, that is, a fixed fraction of the incident solar radiative flux F_0. The flux estimate and its associated error are computed directly from the number of photons N_r that contribute to the radiative flux from a total of N_0 incident photons being simulated.

Normalizing the incident flux $F_0 \equiv 1$, the quantity $1/N_0$ represents the single photon flux quantum. If P is the probability that an incident photon will contribute to the flux being estimated, then that flux must be $F_r = PF_0 = P$. The Monte Carlo estimate for this flux is given by the ratio N_r/N_0. The expected variance of this ratio is computed as usual for N_0 Bernoulli trials each of probability P, as $P(1 - P)/N_0$. Substituting the estimate $P \rightarrow N_r/N_0$ gives this variance as $N_r(N_0 - N_r)/N_0^3$. The ratio of this standard deviation to the computed flux defines the relative error in the flux, which gives

$$E_r = \left(\frac{1-P}{N_0 P}\right)^{1/2} \approx \left(\frac{1-P}{N_r}\right)^{1/2} \approx \left(\frac{N_0 - N_r}{N_0 N_r}\right)^{1/2}, \tag{B1}$$

showing the usual $\sim N_r^{-1/2}$ relationship. The relative error is determined directly by the number N_r of photons that contribute. From this relationship it is clear that, if the estimated flux is a very small fraction of the incident flux, that is, $P \ll 1$, the number of incident photons N_0 must be quite large.

Fortunately, area-averaged hemispherical radiative fluxes are well estimated by the simulation process. In estimating the reflected flux from a cloud field, for instance, P is equal to the cloud field albedo, which is not small compared to unity. For example, if one performs a typical short simulation for a homogeneous cloud of 2^{12} cells with albedo 0.5, 100 incident photons might be directed at each cloud cell for a total $N_0 = 409\,600$. Estimates of the local reflectivity for any single cell would have a relative error of about 10%. However, the mean cloud field albedo computed from the same simulation has a statistical error 64 times smaller or about 0.2%. A realistic simulation using 6.25

million photons would compute the cloud field albedo to within 0.04%, giving a result of 0.5000 ± 0.0002.

If one requires more detailed spatial and directional information, however, the quality of the radiation estimate will be degraded as $P \approx N_r/N_0$ becomes smaller with fewer photons contributing. If one chooses to "zoom in" for very detailed measurement of the angular or spatial dependence of the radiation field at cloud top, for instance, one must rely on contributions from relatively rare events. Using the direct method these estimates are noisy and require a large number of photons at the outset for acceptable statistical error. An alternative for obtaining detailed spatial or angular information is to use variance reduction methods designed to focus computational resources on the small percentage of photons that are likely to contribute. However, because we are most interested in cloud field albedo and radiative fluxes, we have, for the purposes of this study, limited ourselves to the direct method.

b. *Fractal model statistical errors*

The inhomogeneous cloud problem requires specification of a horizontal scale for the width of individual cloud cells. If the scale is large, the radiative transfer problem becomes simply 2^{12} decoupled homogeneous cloud problems. This is the limit where the independent pixel approximation applies exactly. At the other extreme, if the cell width is small in terms of photon mean free paths, photons cross many cell boundaries and they will sample a distribution of local opacities. We are interested in estimating both the cloud field albedo and the apparent brightness of individual cells or clusters of cells for a range of cell horizontal scales.

The cloud field is assumed to be uniformly illuminated. It can be shown that sampling error for estimating total cloud field albedo is reduced if each cloud cell is illuminated with a number of photons proportionate to the total. We treat the problem as $M = 2^{12}$ parallel simulations and count photons exiting from the top of each cloud cell irrespective of the cell where each was incident. We assume that $N_0^i = N_0/M$ photons illuminate each of the M cells and that P^i is the probability that a photon illuminating the ith cell contributes to the albedo by emerging from cloud top. The cloud field albedo A is given by

$$A = \frac{1}{M}\sum_i P^i \equiv P, \qquad \text{(B2)}$$

with total variance V given by

$$V = \frac{1}{M^2}\sum_i \frac{P^i[1 - P^i]}{N_0^i} \leqslant \frac{P[1 - P]}{N_0}. \qquad \text{(B3)}$$

The latter inequality is an equality if all $P^i = P$, which is true in the homogeneous cloud limit only. For the inhomogeneous fractal cloud model

$$E_r \approx \left(\frac{N_0 - N_r}{N_0 N_r}\right)^{1/2}$$

represents an upper bound on the relative error.

In estimating the brightness or apparent albedo from a single cell k when all cells are uniformly illuminated, $P^k \ll 1$ so that the error ratio $E_k \approx N_k^{-1/2}$, but N_k will be a very small fraction of N_0. A better estimate of the local brightness comes from grouping 16–64 cells together in order to reduce the error ratio by a factor of 4–8 or more.

REFERENCES

Barker, H. W., 1992: Solar radiative transfer through clouds possessing isotropic variable extinction coefficient, *Quart. J. Roy. Meteor. Soc.*, **118,** 1145–1162.

——, and J. A. Davies, 1992: Cumulus cloud radiative properties and the characteristics of satellite radiance wavenumber spectra. *Remote Sens. Environ.*, **42,** 51–64.

Cahalan, R. F., 1989: Overview of fractal clouds. *Advances in Remote Sensing Retrieval Methods,* A. Deepak, H. Fleming, and J. Theon, Eds. A. Deepak, 371–388.

——, and J. H. Joseph, 1989: Fractal statistics of cloud fields. *Mon. Wea. Rev.*, **117,** 261–272.

——, and J. B. Snider, 1989: Marine stratocumulus structure. *Remote Sens. Environ.*, **28,** 95–107.

——, and W. J. Wiscombe, 1993: Impact of cloud structure on climate. *Current Problems in Atmospheric Radiation,* S. Keevalik, and O. Kärner, Eds., A. Deepak, 120–124.

——, M. Nestler, W. Ridgway, W. J. Wiscombe, and T. L. Bell, 1990: Marine stratocumulus spatial structure. *Proc. Fourth Int. Meeting on Statistical Climatology,* Wellington, New Zealand, New Zealand Meteorological Service, 28–32.

——, W. Ridgway, W. J. Wiscombe, T. L. Bell, and J. B. Snider, 1994: The albedo of fractal stratocumulus clouds. *J. Atmos. Sci.*, **51,** 2434–2455.

——, 1994: Bounded cascade clouds: Albedo and effective thickness. *Nonlinear Proc. Geophys.*, **1,** 156–157.

Chandrasekhar, S., 1960: *Radiative Transfer.* Dover, 393 pp.

Coakley, J. A., and T. Kobayashi, 1989: Broken cloud biases in albedo and surface insolation derived from satellite imagery data. *J. Climate,* **2,** 721–730.

Davies, R., 1978: The effect of finite geometry on the three-dimensional transfer of solar irradiance in clouds. *J. Atmos. Sci.*, **35,** 1712–1725.

——, W. L. Ridgway, and K.-E. Kim, 1984: Spectral absorption of solar radiation in cloudy atmospheres: A 20 cm^{-1} model. *J. Atmos. Sci.*, **41,** 2126–2137.

Davis, A., A. Marshak, W. J. Wiscombe, and R. F. Cahalan, 1994: Multifractal characterizations of non-stationarity and intermittency in geophysical fields, observed, retrieved, or simulated. *J. Geophys. Res.*, **99,** 8055–8072.

Evans, K. F., 1993: Two-dimensional radiative transfer in cloudy atmospheres: The spherical harmonic spatial grid method. *J. Atmos. Sci.*, **50,** 3111–3124.

Gabriel, P. M., S.-C. Tsay, and G. L. Stephens, 1993: A Fourier–Riccati approach to radiative transfer. Part I. Foundations. *J. Atmos. Sci.*, **50,** 3125–3147.

Gage, K. S., and G. D. Nastrom, 1986: Theoretical interpretation of atmospheric wavenumber spectra of wind and temperature observed by commercial aircraft during GASP. *J. Atmos. Sci.*, **43,** 729–740.

Hansen, J. E., 1971: Multiple scattering of polarized light in planetary atmospheres. Part I. The doubling method. *J. Atmos. Sci.*, **36,** 508–518.

——, and L. D. Travis, 1974: Light scattering in planetary atmospheres. *Space Sci. Rev.*, **16,** 527–610.

Harshvardhan, 1991: Atmospheric radiation. *Rev. Geophys. Suppl.*, U.S. Natl. Rep. to Int. Union Geod. Geophys. 1987–1990, 56–68.

——, and D. A. Randall, 1985: Comments on "The parameterization of radiation for numerical and climate models." *Mon. Wea. Rev.*, **113,** 1832–1833.

House, L. L., and L. W. Avery, 1969: The Monte Carlo technique applied to radiative transfer. *J. Quant. Spectrosc. Radiat. Transfer,* **9,** 1579–1591.

Kattawar, G. W., 1979: Monte Carlo methods in radiative transfer. (Unpublished manuscript.)

King, M. D., 1983: Number of terms required in the Fourier expansion of the reflection function for optically thick atmospheres. *J. Quant. Spectrosc. Radiat. Transfer,* **30,** 143–161.

Kobayashi, T., 1991: Reflected solar flux for horizontally inhomogeneous atmospheres. *J. Atmos. Sci.,* **48,** 2436–2447.

Lovejoy, S., A. Davis, P. Gabriel, D. Schertzer, and G. L. Austin, 1990: Discrete angle radiative transfer. 1. Scaling and similarity, universality and diffusion. *J. Geophys. Res.,* **95,** 11 699–11 715.

Marchuk, G., G. Mikhailov, M. Nazaraliev, R. Darbinjan, B. Kargin, and B. Elepov, 1980: *The Monte Carlo Method in Atmospheric Optics.* Springer-Verlag, 208 pp.

Marshak, A., A. Davis, R. F. Cahalan, and W. J. Wiscombe, 1994: Bounded cascade models as non-stationary multifractals. *Phys. Rev.*, **E49,** 55–69.

McKee, T. B., and S. K. Cox, 1974: Scattering of visible radiation by finite clouds. *J. Atmos. Sci.,* **31,** 1885–1892.

Mullamaa, Y. R., M. A. Sulev, V. K. Poldmaa, H. A. Ohvril, H. J. Niylisk, M. I. Allenov, L. G. Tchübakov, and A. F. Kuusk, 1975: Stochastic structure of cloud and radiation fields. NASA Tech. Transl. F-822, 192 pp. [NTIS 76-N11605.]

O'Brien, D. M., 1992: Accelerated quasi Monte Carlo integration of the radiative transfer equation. *J. Quant. Spectrosc. Radiat. Transfer,* **48,** 41–59.

Press, W. H., B. P. Flannery, S. A. Teukolsky, and W. T. Vetterling, 1992: *Numerical Recipes in C.* Cambridge University Press, 735 pp.

Ronnholm, K., B. Baker, and H. Harrison, 1980: Radiative transfer through media with uncertain or variable parameters. *J. Atmos. Sci.,* **37,** 1279–1290.

Stephens, G. L., 1988a: Radiative transfer through arbitrarily shaped optical media. Part I: A general method of solution. *J. Atmos. Sci.,* **45,** 1818–1836.

——, 1988b: Radiative transfer through arbitrarily shaped optical media. Part II: A group theory and simple closures. *J. Atmos. Sci.,* **45,** 1837–1848.

——, P. M. Gabriel, and S.-C. Tsay, 1991: Statistical radiative transport in one-dimensional media and its application to the terrestrial atmosphere. *Trans. Theor. Stat. Phys.,* **20,** 139–175.

Weinman, J. A., and Harshvardhan, 1982: Solar reflection from an array of horizontally finite clouds. *Appl. Opt.,* **21,** 2940–2944.